Editors' Suggestion

Interferometry with few photons

Q. Pears Stefano,[1,2,*,‡] A.G. Magnoni,[3,1,†] D. Rodrigues,[1,4] J. Tiffenberg,[5] and C. Iemmi[1,2]

[1] *Universidad de Buenos Aires, Facultad de Ciencias Exactas y Naturales, Departamento de Física, Pabellón I, Ciudad Universitaria (1428), Buenos Aires, Argentina*

[2] *Consejo Nacional de Investigaciones Científicas y Técnicas (CONICET)—Universidad de Buenos Aires (1425), Buenos Aires, Argentina*

[3] *Laboratorio de Óptica Cuántica, Departamento de Investigaciones en Láseres y sus Aplicaciones (DEILAP), Unidad de Investigación y Desarrollo Estratégico para la Defensa (UNIDEF) (CITEDEF-CONICET) (B1603ALO), Buenos Aires, Argentina*

[4] *CONICET—Universidad de Buenos Aires, Instituto de Física de Buenos Aires (IFIBA) (1428), Buenos Aires, Argentina*

[5] *Fermi National Accelerator Laboratory, Batavia, Illinois FMPCODE60510, USA*

(Received 22 February 2024; revised 13 May 2024; accepted 13 May 2024; published 21 June 2024)

Optical phase determination is an important and established tool in diverse fields such as astronomy, biology, or quantum optics. There is increasing interest in using a lower number of total photons. However, different noise sources, such as electronic readout noise in the detector, and shot noise, hamper the phase estimation in regimes of very low illumination. Here, we report a study on how the quality of phase determination is affected by these two sources of noise. To that end, we experimentally reconstruct different wave fronts by means of a point-diffraction interferometer for different mean intensities of illumination, up to 15 photons per pixel. Our interferometer features a skipper-CCD sensor, which allows us to reduce the readout noise arbitrarily, thus enabling us to separate the effect of these two sources of noise. For two cases of interest—a spatial qudit encoding phase, consisting of $d = 6$ uniform phase regions, and a more general continuous phase—we see that reducing the readout noise leads to a clear improvement in the quality of reconstruction. This can be explained by a simple noise model that allows us to predict the expected fidelity of reconstruction and shows excellent agreement with the measurements.

DOI: 10.1103/PhysRevApplied.21.064050

I. INTRODUCTION

Interferometric measurements of light involve different techniques that allow to know phase distributions with high precision. Although interferometry was initially related to metrology of optical systems, its applications have spread into fields as diverse as astronomy, biology, quantum optics, and many more. Current advances achieved in computers and optoelectronic devices, such as spatial light modulators and detectors, make interferometry a widely used tool in a large number of applications [1–6].

Digital recording and numerical processing of an interferogram has led to a great improvement in measurement techniques. It was not until the mid-1990s that light sensors began to provide images of a certain quality. But, once the initial objective was achieved, which was to increase their spatial resolution, the challenge of achieving images with low light levels and good signal-to-noise ratio (SNR) arose.

Two sources of noise corrupt the process of capturing an image: those that come from the source (shot noise) and those that originate from the sensor (readout noise). Even though increasing the signal (either the intensity or the exposure time) seems an obvious way to improve the SNR, there are experiences where this is not possible. Some alternative proposals include the use of unconventional light sources such as squeezed states or entangled photons [7,8]. Unfortunately, these devices are not easy to implement in most optical setups. Measurements at very low light levels have applications in diverse fields, including quantum information processing or biological studies, where the sample can be damaged by a high photon flux. Some of these experiences can be performed by using, e.g., a highly attenuated laser beam. In that scenario, a doubt arises: how many photons are needed to calculate a phase distribution? In order to answer that question, it

*Corresponding author: quimeymartin.pearsstefano@ehu.eus
†Corresponding author: magnoni.agustina@gmail.com
‡Present address: Centro de Física de Materiales, Paseo Manuel de Lardizabal 5, 20018 Donostia-San Sebastián, Spain.

would be necessary to be able to separate the noise caused by the light-source statistics from the readout noise. A direct way of doing this is by eliminating the latter using a skipper-CCD sensor [9], which, by contrast with other technologies, offers this feature over an unprecedentedly wide dynamic range, from zero to a 1000 photons per pixel [10]. In this work, we propose to measure phase distributions at very low light levels in two different situations. In one of them, we perform quantum state tomography (QST) on spatial qudits (that is D-level quantum systems). In the other, we evaluate an arbitrary phase distribution: in this case, we evaluate a continuous quadratic wave front. The phase reconstruction process is analyzed for different numbers of photons per pixel and readout noise on the skipper CCD.

The paper is organized as follows. in Sec. II, we review the interferometric process used to obtain the phase distribution, while in Sec. III we describe the experimental setup. In Sec. IV, on the one hand, we numerically simulate the expected results for different light intensities, taking into account the light-source statistics and the readout noise. On the other, the data-acquisition method is explained and the experimental results are analyzed. Finally, in Sec. V we give the conclusions.

II. METHODOLOGICAL FRAMEWORK

Phase-shifting interferometry (PSI) has proven to be an accurate and precise method to evaluate wave-front phase distributions. In this technique, controlled phase shifts are introduced between the reference and the tested beam [11]. The number of interferograms recorded as the phase is shifted varies depending on the algorithm employed to recover the phase distribution of the wave front.

As it has previously been mentioned, to diminish the readout noise, we have used a skipper CCD. Although this device requires a recording time similar to that of conventional CCDs, the total acquisition time for each interferogram, including the noise-reduction process, of (60 μs per pixel per sample), makes necessary the use of a very stable interferometer. To this end, we have implemented an architecture based on a point-diffraction interferometer (PDI) that was introduced by Linnik [12]. Its common-path configuration, where the reference beam is generated from the same wave front under characterization, results on an interferometer that is extremely stable against vibrations and air turbulence. When combined with PSI schemes by, e.g., using liquid-crystal technology [13–15] to control the phase steps, the potential applications of this interferometer are enhanced, as these schemes can perform accurate phase reconstruction by acquiring only a few interferograms. Furthermore, the pixel-by-pixel control of phase provided by liquid-crystal spatial light modulators (SLMs) allows us to introduce the phase steps in the pointlike geometry required by the PDI.

The reconstruction of the full wave front $U(x,y)$ is done by using a PSI architecture similar to that described in Ref. [14]. Briefly, a convergent optical processor allows us to apply, at the Fourier-transform plane of the input wave front $U(x,y)$, a pointlike phase filter. This element generates a diffracted beam that is used as the interferometric reference. The resulting interferograms of applying $N = 4$ controlled phase shifts, $\alpha_n = 2\pi n/N$, with $n = 0,\ldots,3$, are registered with the skipper CCD.

The resulting amplitude for each of the phase shifts α_n at the image plane Π_i is

$$E_n(x,y) = U(x,y) + |K|e^{i\mu}\left[e^{i\alpha_n} - 1\right], \tag{1}$$

where $|K|$ and μ are, respectively, the amplitude and phase of the reference beam. It is worth noting that the reference beam corresponds to a plane wave with the mean value of $U(x,y)$. To highlight that the final aim of this method is to obtain the phase of $U(x,y)$, it is useful to rewrite $U(x,y) = u(x,y)\exp(i\phi(x,y))$, where $u(x,y)$ is the absolute value of $U(x,y)$ and $\phi(x,y)$ represents the phase. With the aid of the following combination of all the interferograms,

$$C(x,y) = \sum_{n=0}^{N} |E_n(x,y)|^2 \cos\left(\frac{2\pi n}{N}\right), \tag{2}$$

$$S(x,y) = \sum_{n=0}^{N} |E_n(x,y)|^2 \sin\left(\frac{2\pi n}{N}\right), \tag{3}$$

the unknown phase of the wave front $\phi(x,y)$ can be reconstructed as

$$\phi(x,y) = \arctan2(S, C - C_0) - \mu, \tag{4}$$

where $\arctan2(x_1,x_0)$ is defined as the angle between the two-dimensional vector (x_0,x_1) and the x_0 axis and $C_0 = -N|K|^2$. The value of C_0 can be readily obtained from the value of $C(x,y)$ at the points in which the input wave front $U(x,y)$ is zero. Finally, the real amplitude of $u(x,y)$ is E_0.

III. EXPERIMENTAL SETUP

The experimental setup, sketched in Fig. 1, is basically a convergent optical processor, where two phase-only SLMs are used: one to display the phase distribution to be measured, $U(x,y)$, and the other to dynamically introduce the phase retardation needed to implement the PSI process. The light source is a laser diode at 405 nm, which is expanded by the microscope objective O and spatially filtered by a pinhole that is imaged by lens $L1$ onto the Fourier plane Πf . The phase distribution $U(x,y)$ is displayed on the phase-only SLM1, which is placed at the object plane Πo. When $U(x,y)$ is uniform, the resulting

light distribution on Πf is a bright central spot, corresponding to the Fourier transform of the entrance pupil of the system. At this position, a phase filter $H(u, v)$, smaller than the focused spot, is displayed on SLM2. Then the phase shifts α_n needed to implement the PSI technique are introduced in the central pixel. (see inset in Fig. 1). This pixel is used as a perturbation to generate a spherical wave by diffraction. When the phase distribution $U(x, y)$ is not uniform, the bright spot is deformed. Most of the light is diffracted toward higher spatial frequencies and only the small central part of the spot goes through the phase filter. After SLM2, the lens $L2$ is placed at a distance equal to its focal length $f\,2$ and images the object plane onto Πi. In this way, the spherical reference wave front, which is diffracted by the central pixel, is collimated and interferes with the tested wave front. Finally, the interferograms are detected by the skipper CCD placed at the image plane Πi. The main advantage of this convergent configuration is that it allows us to change the size of the Fourier transform, to better suit the size of the PDI filter.

Both SLMs are conformed by a Sony liquid-crystal television panel model LCX012BL which, in combination with polarizers and wave plates, that provide the adequate state of light polarization, allows a 2π phase modulation [16]. These liquid-crystal displays have a video graphics array (VGA) resolution of 640×480 and a pixel size of 43 μm. Although the skipper CCD has hitherto only been used as a particle detector [10,17–20], in a recent paper [21] it has been used for imaging purposes. This device offers ultralow readout noise and photon-number-resolving capability. These features are achieved by eliminating the low-frequency readout noise (around 2 e^- in a conventional CCD) by multiple nondestructive measurements (samples) of the charge in each pixel. For a readout noise of 0.2 e^- (attained after 256 samples), the photon-counting probability of misclassification is lower than 1% and can be further reduced just by increasing the number of charge samples [10]. This technology also provides the lowest dark current (approximately 10^{-4} e^- per pixel per day) [20] and a full-well capacity above 33 000 electrons [22] in a spatially resolved sensor with only a (15×15) μm pixel size. The skipper-CCD sensor has a total active area of 4126×886 pixels. It was designed at the Lawrence Berkeley National Laboratory and manufactured by Teledyne-DALSA using high-resistivity (>10-kΩ cm) silicon wafers. As it operates in the temperature range of 135–140 K, in vacuum, the sensor is placed into a vessel that has a fused silica window (W). A dark chamber composed of a black-painted metallic holder is firmly attached to the skipper-CCD vessel. This holder is used to place a Melles Griot electronic shutter (S), which allows us to control the light exposure, and a square interferential filter (IF) centered at the laser wavelength, thus avoiding spurious ambient light from entering the sensor. Additionally, neutral filters (NFs) are employed in order to reduce the light intensity.

After the exposure to the light for each of these phase steps, the reading process begins. This can be done in an efficient way by selecting the number of charge samples, NSAMP, desired for each region of the sensor, thus optimizing the total readout time of the measurement. The raw outcome is data in analog-to-digital units (ADUs) for each pixel that needs to be calibrated to the number of electrons. Since the readout noise can be reduced to subelectron values for a high NSAMP, there is a closed relation between these two variables with very low probability of misclassification. The complete process for this calibration is described in Refs. [10,21].

IV. NUMERICAL SIMULATIONS AND EXPERIMENTAL RESULTS

At very low light levels, two independent problems arise. On the one hand, the fluctuations in the number of photons become comparable to the average number of photons, so that the noise coming from the light-source statistics affects the accuracy of the phase estimation. On the other, the average number of photons is itself comparable to the readout noise of the camera used to acquire the interferograms. Thus, it is of interest to study, under these conditions, what is the average minimum number of photons per pixel that is necessary to carry out the phase-reconstruction process with a certain degree of reliability and, furthermore, how this number depends on the readout noise of the camera.

In this work, we have explored two cases of interest: the discrete phase representing a qudit in the codification of *slit states* and a continuous quadratic phase representing a convergent lens.

A. Slit states

The first case is specially relevant for quantum information tasks. The slit states, the formalism of which is described in detail in Refs. [23–25], are a versatile codification that harnesses the spatial degrees of freedom of a single photon, to allow the creation of high-dimensional quantum states. In particular, the discretized transverse momentum of single photons defines photonic quantum states. In a previous work, we have shown [26] how to characterize these slit states with a PDI interferometric configuration.

In Fig. 2(a), we show schematically the phase distribution that represents the slit states. They consist of a phase mask with d rectangular slits of width a and length $L(\gg a, s)$, where the separation between adjacent slits is s.

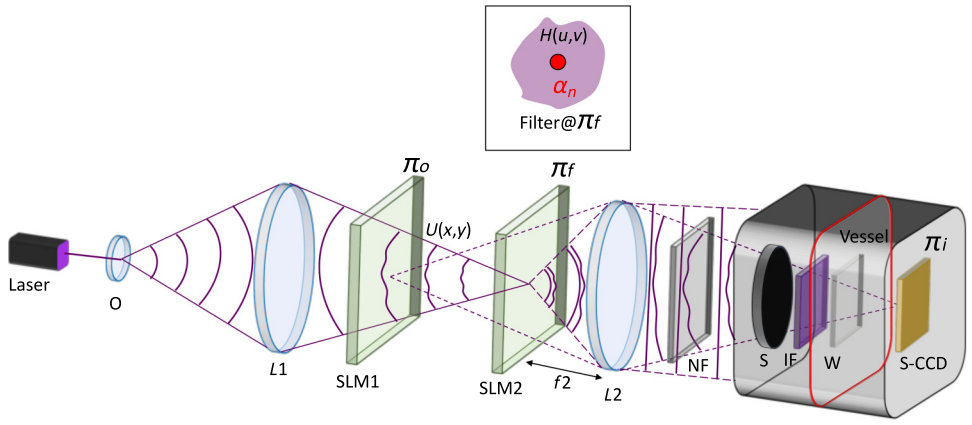

FIG. 1. The experimental setup. The light source is a 405-nm cw laser diode, attenuated down to the single-photon level. The lenses *Ls* conform to a convergent optical processor. The SLMs are phase-only spatial light modulators. The interferograms are detected by a skipper CCD. The detail shows the filter placed at the Fourier plane Πf, where the central pixel of SLM2 introduces the PSI phase retardation α_n.

Thus, the resulting state is

$$|\Psi\rangle = \sum_{k=0}^{d-1} c_k |k\rangle, \tag{5}$$

where $\{|k\rangle\}_{k=0}^{d-1}$ is the logical basis and the complex coefficients c_k represent the transmissivity and phase of each of the slits. Additionally, in order to have a light distribution similar to those usually present in an in-line holography process (small diffracting objects immersed in a strong background), we embed these slits in a constant light background with uniform phase. This has the additional benefit that the information of the phase reconstructed on the background could be utilized to improve the state determination in the presence of optical aberrations, such as the ones induced by turbulence in free-space propagation [26].

As in this work we are focusing in phase determination, we choose a single particular state with uniform intensity in each slit, of dimension $d = 6$, and with a phase that increases in equal steps between adjacent slits:

$$|\Psi\rangle = \frac{1}{\sqrt{6}} \sum_{k=0}^{d-1} \exp(i2\pi k/5)|k\rangle. \tag{6}$$

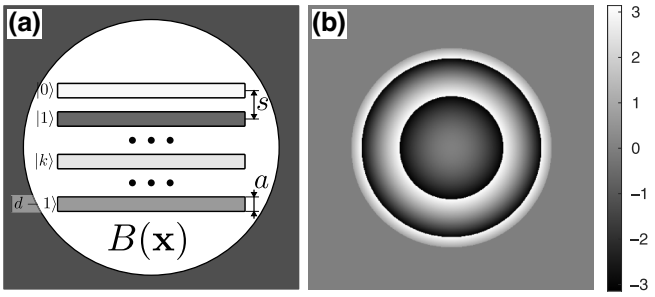

FIG. 2. The programmed phases in the first SLM: (a) the slit photonic qudit state case; (b) the Continuous lenslike phase map.

Thus, our target state contains optical phases in all the range between 0 and 2π and this single state would allow us to evaluate the performance of the phase reconstruction in the full phase range.

Once the phase of each pixel is estimated by Eq. (4), as described in Sec. II, the state is reconstructed at random by one pixel corresponding to each of the slits and assigning that phase value to that element of the canonical basis. As a figure of merit, we have used the fidelity, which is defined, for pure states, as $F(\Phi, \Psi) = |\langle\Phi|\Psi\rangle|$, where $|\Phi\rangle$ represents the state to be prepared and $|\Psi\rangle$ the state that is reconstructed [27].

We have reconstructed the state given by Eq. (6) for three levels of illumination—1.7, 3.0, and 11.3 photons per pixel—that have been acquired with an exposure time of 1/30, 1/30, and 1/60 s, respectively, where the illumination has been estimated as the intensity averaged over all the pixels in the region defined by the slits (approximately 600). However, in order to study other values of illumination, we have considered the *n*-pixel (binning of *n* pixels) averaged state, where the state determination has been made by averaging the phase for *n* randomly chosen pixels in the region of each of the slits. In this case, we have defined the effective illumination as being *n* times the real illumination per pixel. To estimate the mean value of the fidelity and its spread in each case, we have performed a bootstrap method: for each level of noise and binning *n*, we have sampled, without repetition, 81 *n*-binned reconstructions of the target state, to

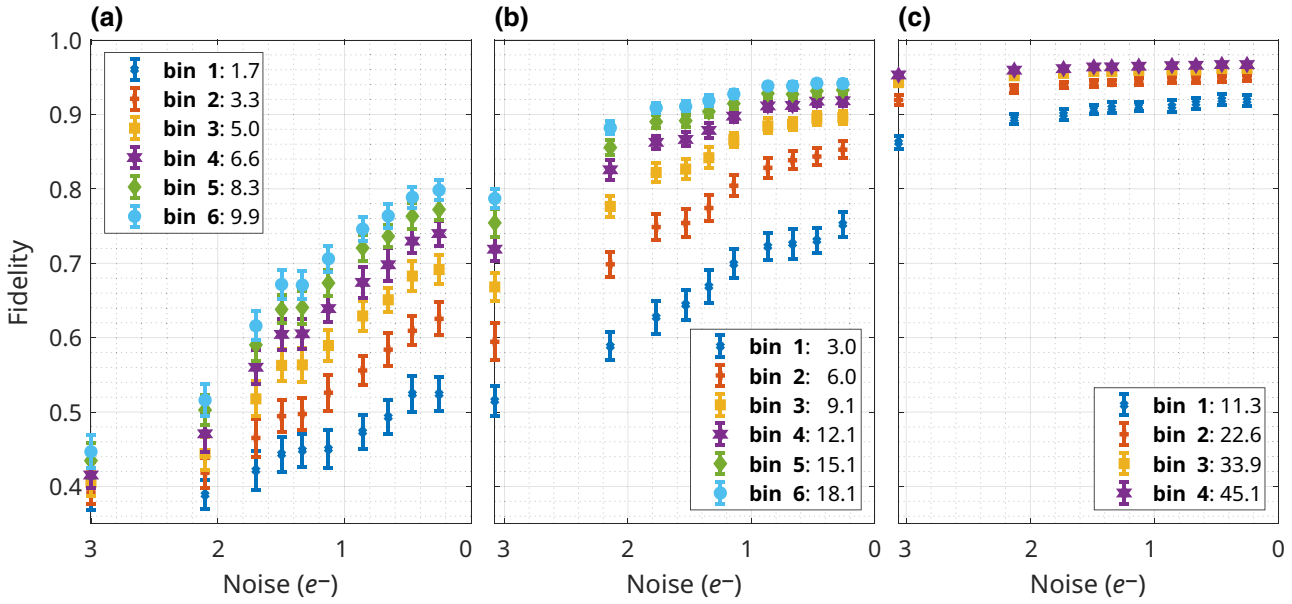

FIG. 3. The reconstruction fidelity as a function of the readout noise, for three different effective illuminations: (a) 1.7, (b) 3.0, and (c) 11.3 photons per pixel. The different curves represent effective illuminations, where the state has been estimated by selecting, at random, n pixels for each slit.

obtain an average fidelity. As part of the bootstrap estimation, this process has been repeated 64 times to obtain the mean value of these averaged fidelities and its standard deviation.

In Fig. 3, we show how the reconstruction fidelity changes with the readout noise, for the three cases of real illumination. Each of the curves in a single plot represents the effective illumination that was obtained by binning n pixels for each of the slit regions, to determine the phase of said slit. The improvement in the fidelity attained by increasing the number of samples in the skipper-CCD mode is clear from these plots. The highest readout noise corresponds to NSAMP = 1 samples in the skipper CCD (approximately 3 e^-), while the smallest readout noise corresponds to NSAMP = 144 samples (approximately 0.2 e^-).

In all cases, the reduction in the readout noise leads to an increase in the fidelity reconstruction. However, for the lowest level of illumination, 1.7 photons per pixel, the maximum achieved fidelity for one bin is about 0.5, indicating that this number of photons is not sufficient to determine the phase. The fidelity in this case can be improved by averaging the phase over more pixels and thus incrementing the effective illumination. However, there is a striking difference compared to the other two levels of illumination. For 3.0 photons per pixel, the one-bin case can achieve more than 0.75 fidelity when readout noise is decreased well below 1 e^-. Also, a binning greater or equal to 2 is enough to obtain mean reconstruction fidelities over 0.8, for the same readout-noise condition. In the last case, with over 11 photons per pixel, the worst-case scenario corresponds to a fidelity that is already over 0.85 and the improvements are smaller both with the increased binning and the decrease in the readout noise. It is to be expected that both the relative effect of Poissonian fluctuations and that of the readout noise are much smaller.

1. Simulation

To perform the simulation, for each configuration of light level, synthetic interferograms have been generated

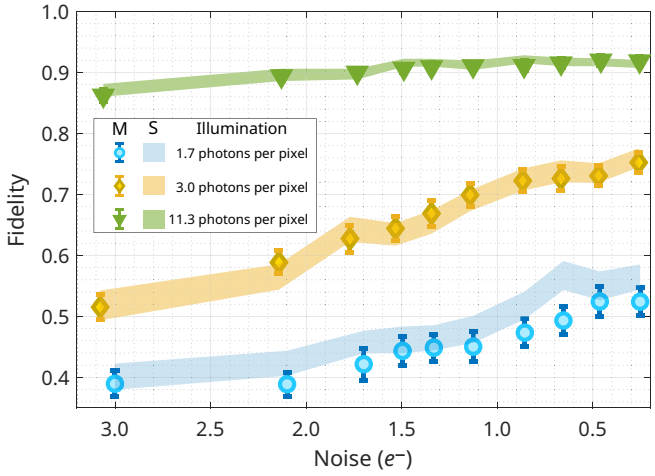

FIG. 4. The measured (M, error bar) and simulated (S, shaded area) fidelities as a function of the readout noise for three different illuminations. The error bars represent the standard error over 100 realizations of the selection of the pixels in the region of interest of each slit.

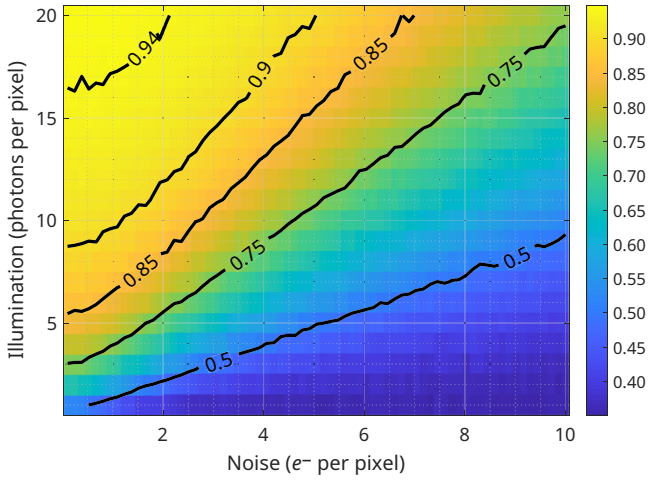

FIG. 5. A simulated map of the mean fidelity as a function of the total illumination and the readout noise.

according to Eq. (1). To account for the Poissonian-noise characteristic of the photon statistic of a highly attenuated coherent state, we have sampled, for each of the pixels of each of the interferograms, a Poissonian distribution with the mean value corresponding to the intensity value of said pixel. Also, additional Gaussian noise is added to each pixel, with zero mean and a standard deviation equal to the electronic noise, to represent the readout noise of the camera.

In Fig. 4, we compare the measured and the simulated fidelity reconstruction as a function of the readout noise of the camera, for three different examples of illumination: 1.7, 3.0, and 11.3 photons per pixel. In this case, the binning was $n = 1$ and the random sampling was repeated 100 times. The continuous line represents the average fidelity over the repetitions, while the error bars represent the standard error. On the other hand, the point represents the simulated reconstruction fidelity, averaged over 2000 repetitions. For the two highest illuminations, the noise model is in excellent agreement with the measurements. In the case of the lowest illumination level, the simulated mean fidelity is consistently above the value estimated experimentally but the confidence band overlaps for most of the points.

Thus, this noise model is a useful tool to estimate what the expected reconstruction fidelity is, given the level of illumination and the readout noise of the detector used. In that regard, in Fig. 5 we show the mean fidelity map as a function of the electronic noise and the mean illumination, where each point is an average over 2000 repetitions. To assess this fidelity for another dimension, a similar map can be generated using the same statistical model.

It should be noted that our analysis is based on raw images, i.e., we do not use maximum-likelihood algorithms [28] to improve them, nor do we apply principles of image compression and associated image reconstruction [29]. We also do not improve the sensitivity of the measurement by using photon-subtracted thermal states [30].

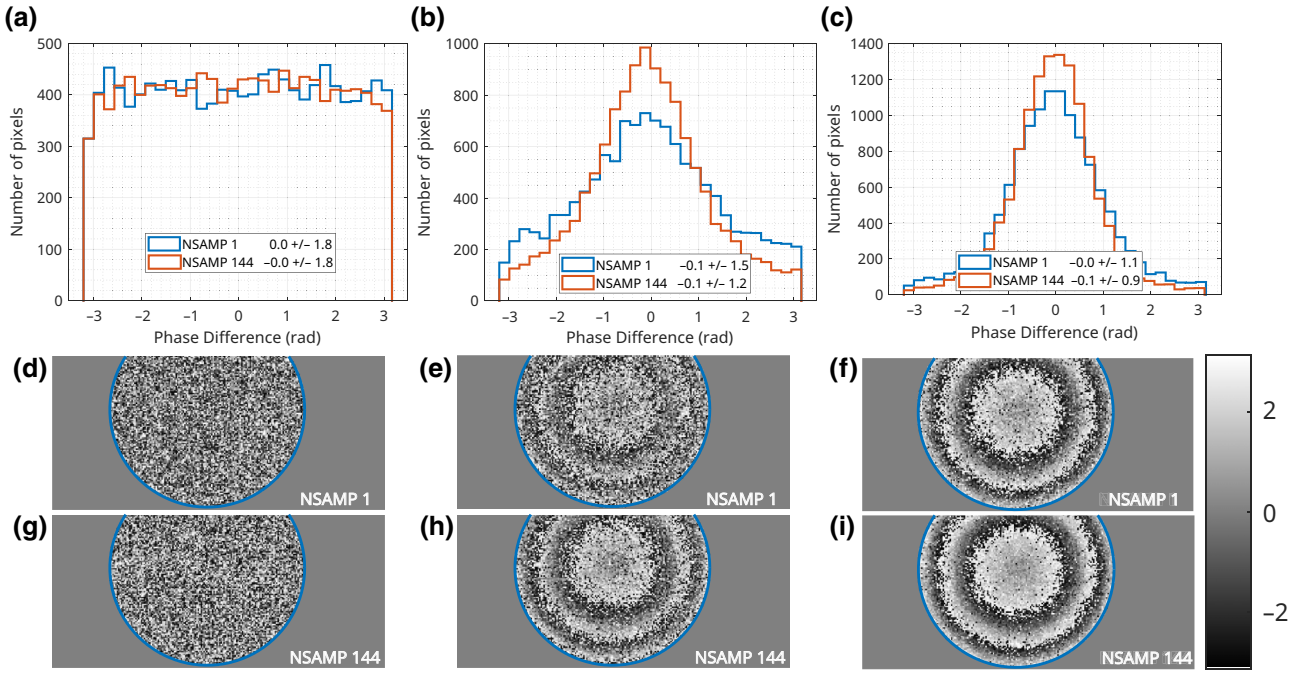

FIG. 6. Each column shows, for a fixed illumination intensity, the histogram of the phase difference in each pixel for a lenslike phase wave front (top row) and the corresponding phase map for NSAMP = 1 (middle row), and for NSAMP = 144 (bottom row): (a),(d),(g) 1.9, (b),(e),(h) 4.0, and (c),(f),(i) 12.7 photons per pixel.

B. Measurement of an arbitrary phase distribution

Another case of interest is that of the determination of an arbitrary phase distribution. In order to study this case, we have programmed in the SLM1 a lenslike phase, i.e., a quadratic phase, as represented schematically in Fig. 2(b).

As in this case we cannot define regions of constant phase, to assess the quality of the phase reconstruction, we compare the obtained phase map with a reference one, which has been obtained with high light intensity (approximately 500 photons per pixel, where both the Poissonian and the readout noise are negligible).

The upper row of Fig. 6 shows the histogram of the phase differences for three different illuminations—1.9, 4.5, and 12.7 photons per pixel—and the two lines in each histogram correspond to the measurement without the skipper-CCD mode (NSAMP = 1) and with the skipper-CCD mode (NSAMP = 144). The lower rows show a comparison between the reconstructed phase maps for the minimum (NSAMP = 1, medium row) and the maximum (NSAMP = 144, bottom row) number of skipper-CCD samples that we have used. It is worth noting that the quality of the reconstruction for 1.9 photons per pixel [Fig. 6(a)] does not improve even when reducing the readout noise well below the 1-e^- level. This is consistent with the results that we have obtained in the discrete case [Fig. 3(a) – bin 1], where with approximately the same level of illumination, the reconstruction fidelity could not be increased by more than approximately 0.5.

Instead, for the cases of Figs. 6(b) and 6(c), there is a improvement in the phase estimation with the number of skipper-CCD samples, reflected in a decrease of approximately 20% in the standard deviation of the phase difference. In these two cases, a clear improvement in the phase map can be seen as the readout noise is reduced. However, for the case of 12.7 photons per pixel, the improvement is smaller, as both the readout noise and the Poissonian noise start to be significantly lower than the mean intensity.

Thus, the phase determination can be significantly improved by reducing the readout noise, by taking advantage of the skipper mode, for medium illumination levels; approximately, between four and 15 photons per pixel. Interestingly, even when the readout noise is negligible, as is the case with the skipper-CCD camera, a light level slightly higher than four photons per pixel is still needed to reconstruct phases.

V. CONCLUSIONS

In this work, we have studied how interferometric phase reconstruction is affected by the two main sources of noise for highly attenuated coherent illumination: the readout noise of the detector used to record the interferograms and the shot noise of the illumination.

We have reconstructed the phase of several wave fronts with a combination of a PDI and phase-shifting interferometry, where the detection has been done by skipper-CCD camera, allowing us to select, and even eliminate, the readout noise.

On the one hand, we have performed the reconstruction of a spatial distribution with $d = 6$ uniform phase regions that encode a d-dimensional qudit. In this case, we have shown an improvement in the reconstruction fidelity with the reduction of the readout noise for all the illumination levels. However, even in the absence of readout noise, with under 3 photons per pixel it has not been possible to reconstruct states with a fidelity over 0.8. In this particular case, we propose a noise model to predict the expected fidelity reconstruction as a function of both the readout noise level and the mean number of photons, which is consistent with the experimental results.

On the other hand, we have reconstructed a continuous phase, showcasing phase reconstruction under low illumination for arbitrary phases. In a similar manner to the discrete case, the quality of the reconstruction has been improved by the reduction of the readout noise for illuminations greater than 4 photons per pixel. Likewise, even in the absence of readout noise, a nonmeaningful phase could be estimated with less than 3 photons per pixel.

ACKNOWLEDGMENTS

This work was supported by Fermilab under Department of Energy (DOE) Contract No. DE-AC02-07CH11359. The CCD development work was supported in part by the Director, Office of Science, of the DOE under Contract No. DE-AC02-05CH11231. C.I. and Q.P.S. acknowledge the support of the Secretaría de Ciencia y Técnica, Universidad de Buenos Aires (20020170100564BA), of the Consejo Nacional de Investigaciones Científicas y Técnicas (PIP 2330), and of the Ministerio de Ciencia Tecnologia e Innovacion–Agencia Nacional de Promocion Cientifica y Tecnologica (PICT-2020-SERIEA-02031). Q.P.S. was supported by a CONICET Fellowship.

[1] D. Malacara, *Optical Shop Testing* (Wiley, Hoboken, Nueva Jersey, 2007).

[2] U. Schnars and W. Jüptner, Direct recording of holograms by a CCD target and numerical reconstruction, Appl. Opt. **33**, 179 (1994).

[3] M. K. Kim, Principles and techniques of digital holographic microscopy, J. Photon. Energy **1**, 018005 (2010).

[4] J. Kacperski and M. Kujawinska, Active, LCoS based laser interferometer for microelements studies, Opt. Express **14**, 9664 (2006).

[5] H. Zhang, F. A. Monroy-Ramírez, A. Lizana, C. Iemmi, N. Bennis, P. Morawiak, W. Piecek, and J. Campos, Wavefront imaging by using an inline holographic microscopy system based on a double-sideband filter, Opt. Lasers Eng. **113**, 71 (2019).

[6] Q. Pears Stefano, L. Rebón, S. Ledesma, and C. Iemmi, Determination of any pure spatial qudits from a minimum number of measurements by phase-stepping interferometry, Phys. Rev. A **96**, 1 (2017).
[7] V. Giovannetti, S. Lloyd, and L. Maccone, Standard quantum limit, Science **306**, 1330 (2004).
[8] M. W. Mitchell, J. S. Lundeen, and A. M. Steinberg, Super-resolving phase measurements with a multiphoton entangled state, Nature **429**, 161 (2004).
[9] J. Tiffenberg, M. Sofo-Haro, A. Drlica-Wagner, R. Essig, Y. Guardincerri, S. Holland, T. Volansky, and T.-T. Yu, Single-electron and single-photon sensitivity with a silicon skipper CCD, Phys. Rev. Lett. **119**, 131802 (2017).
[10] D. Rodrigues, K. Andersson, M. Cababie, A. Donadon, A. Botti, G. Cancelo, J. Estrada, G. Fernandez-Moroni, R. Piegaia, M. Senger, M. S. Hao, L. Stefanazzi, J. Tiffenberg, and S. Uemura, Absolute measurement of the Fano factor using a skipper-CCD, Nucl. Instrum. Meth. A **1010**, 165511 (2021).
[11] K. Creath, V phase-measurement interferometry techniques, Prog. Opt. **26**, 349 (1988).
[12] W. P. Linnik, A simple interferometer for the investigation of optical systems, C. R Acad. Sci. URSS **5**, 208-210 (1933).
[13] C. R. Mercer and K. Creath, Liquid-crystal point-diffraction interferometer for wave-front measurements, Appl. Opt. **35**, 1633 (1996).
[14] C. Iemmi, A. Moreno, J. Nicolás, and J. Campos, Evaluation and correction of aberrations in an optical correlator by phase-shifting interferometry, Opt. Lett. **28**, 1117 (2003).
[15] C. Ramírez, E. Otón, C. Iemmi, I. Moreno, N. Bennis, J. M. Otón, and J. Campos, Point diffraction interferometer with a liquid crystal monopixel, Opt. Express **21**, 8116 (2013).
[16] A. Márquez, C. Iemmi, I. Moreno, J. A. Dais, J. Campos, and M. J. Yzel, Quantitative prediction of the modulation behavior of twisted nematic liquid crystal displays based on a simple physical model, Opt. Eng. **40**, 2558 (2001).
[17] L. Barak, *et al.*, SENSEI: Direct-detection results on sub-GeV dark matter from a new skipper CCD, Phys. Rev. Lett. **125**, 171802 (2020).
[18] N. Castelló-Mor (DAMIC-M),DAMIC-M experiment: Thick, silicon CCDs to search for light dark matter, Nucl. Instrum. Meth. A **958**, 162933 (2020).
[19] A. Aguilar-Arevalo *et al.* (CONNIE), Search for coherent elastic neutrino-nucleus scattering at a nuclear reactor with CONNIE 2019 data, J. High Energy Phys. **2022**, 17 (2022).
[20] L. Barak, *et al.*, SENSEI: Characterization of single-electron events using a skipper charge-coupled device, Phys. Rev. Appl. **17**, 014022 (2022).
[21] Q. Pears Stefano, A. Magnoni, J. Estrada, C. Iemmi, D. Rodrigues, and J. Tiffenberg, Infrared photon-number-resolving imager using a skipper charge-coupled device, Phys. Rev. Appl. **19**, 064044 (2023).
[22] A. Drlica-Wagner, E. M. Villalpando, J. O'Neil, J. Estrada, S. Holland, N. Kurinsky, T. Li, G. F. Mooni, J. Tiffenberg, and S. Uemura, Characterization of skipper CCDs for cosmological applications, Proc. SPIE Int. Soc. Opt. Eng. **11454**, 114541A (2020).
[23] L. Neves, S. Pádua, and C. Saavedra, Controlled generation of maximally entangled qudits using twin photons, Phys. Rev. A **69**, 042305 (2004).
[24] M. A. Solís-Prosser, A. Arias, J. J. M. Vaga, L. Rebón, S. Ledesma, C. Iemmi, and L. Neves, Preparing arbitrary pure states of spatial qudits with a single phase-only spatial light modulator, Opt. Lett. **38**, 4762 (2013).
[25] J. J. Varga, S. Ledesma, C. Iemmi, and L. Rebón, Controlled generation of mixed spatial qudits with arbitrary degree of purity, Phys. Rev. A **96**, 34 (2017).
[26] Q. Pears Stefano, L. Rebón, and C. Iemmi, Determination of spatial quantum states by using point diffraction interferometry, J. Opt. **22**, 115201 (2020).
[27] M. A. Nielsen and I. L. Chuang, *Quantum Computing and Quantum Information* (Cambridge University Press, Cambridge, England, 2000).
[28] D. A. Barmherzig and J. Sun, Towards practical holographic coherent diffraction imaging via maximum likelihood estimation, Opt. Express **30**, 6886 (2022).
[29] P. A. Morris, R. S. Asden, J. E. C. Bel, R. W. Bod, and M. J. Pagett, Imaging with a small number of photons, Nat. Commun. **6**, 5913 (2015).
[30] S. M. Hashemi Rafsanjani, M. Mirhosseini, O. S. Magaña-Loaiza, B. T. Gard, R. Birrittella, B. E. Kotenbah, C. G. Paazzoli, B. A. Caron, C. C. Gery, J. P. Doling, and R. W. Bod, Quantum-enhanced interferometry with weak thermal light, Optica **4**, 487 (2017).